Hybrid III-V/Si Distributed-Feedback Laser Based on Adhesive Bonding

Stevan Stanković, *Member*, *IEEE*, Richard Jones, *Member, IEEE*, Matthew N. Sysak, *Member, IEEE*, John M. Heck, *Member*, *IEEE*, Günther Roelkens, *Member, IEEE*, and Dries Van Thourhout, *Member, IEEE*

***Abstract*—A hybrid, evanescently coupled III-V/Silicon distributed-feedback laser with an integrated monitor photodiode, based on adhesive divinyl siloxane-benzocyclobutene bonding and emitting at 1310 nm is presented. An output power of ~ 2.85 mW is obtained in continuous wave (CW) regime at 10 °C. The threshold current is 20 mA and a side mode suppression ratio of 45dB is demonstrated. Optical feedback is provided via corrugations on top of the silicon rib waveguide while a specially developed bonding procedure yields 40nm-thick adhesive bonding layers, enabling efficient evanescent coupling.**

***Index Terms*—Evanescent coupling, heterogeneous integration, distributed-feedback lasers, silicon photonics.**

I. Introduction

SILICON photonics is the most promising technology for industrial-scale fabrication of high-performance photonic integrated circuits (PICs) and their co-integration with electronic devices on a single chip as it is based on the silicon-on-insulator (SOI) material platform and uses the well-established silicon fabrication processes and tools. A light source is an essential element in PICs, but fabrication of an efficient, single-wavelength laser on the SOI platform is challenging due to silicon's indirect bandgap. Heterogeneous integration of III-V materials and SOI waveguides is a promising approach to this problem, offering high-density integration and avoiding the need for costly active alignment required in the case of packaged lasers. Among several types of hybrid III-V/Si lasers, evanescently coupled devices show a great potential for industrial-scale fabrication. Most of the previously demonstrated, evanescently coupled hybrid lasers, including Fabry-Perot [1]-[3], distributed Bragg reflector (DBR) [4], and distributed-feedback (DFB) lasers [5] were based on a molecular (direct) wafer bonding technique which requires ultra-clean, smooth and contamination-free surfaces. Anticipating that such strict requirements might present challenges to industrial-scale fabrication of these lasers, we have focused on an alternative approach based on adhesive bonding, using the commercially available polymer divinyl-siloxane-benzocyclobutene (DVS-BCB).

In recent years, DVS-BCB bonding has been successfully used for the fabrication of hybrid III-V/Si lasers with adiabatic polymer-overlayed inverted tapers [6], narrow-tip spot-size converters [7], as well as microdisk lasers [8]. The adhesive bonding layers in these applications were not always thin enough to be suitable for evanescent hybrid lasers. Recently, a bonding procedure providing less than 100nm-thick DVS-BCB bonding layers between III-V materials and SOI photonic platform has been reported [9], allowing the demonstration of an evanescent hybrid, III-V/Si Fabry-Perot laser at 1310nm [10]. In this letter, we present the design and fabrication of an evanescently coupled, hybrid III-V/Silicon DFB laser operating at 1310 nm, based on DVS-BCB adhesive bonding.

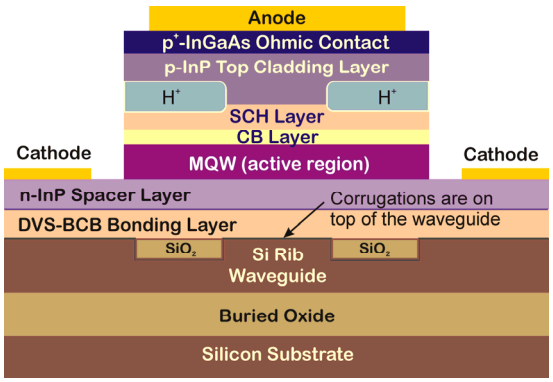

Fig. 1 Cross-section of an evanescent, hybrid III-V/Si DFB laser based on DVS-BCB bonding (SCH: separate confinement heterostructure; CB: carrier blocking; MQW: multi-quantum well). Corrugations are fabricated on top of the Si rib waveguide.

II. Hybrid III-V/Silicon DFB Laser Design

The cross-section of the hybrid III-V/Silicon evanescent laser is shown in Fig. 1. The SOI platform consists of rib Si waveguides of 500 nm height and 0.8 μm width, surrounded by 220 nm deep and 3.5 μm wide trenches. For better SOI wafer uniformity, these trenches are filled with planarized SiO_2, using chemical vapor deposition (CVD), followed by

Manuscript received on August 23, 2012. This work was supported by a grant from Intel Corporation and partly supported by the EU-commission through the ERC-grant ULPPIC.

S. Stanković, G. Roelkens, and D. Van Thourhout are with Photonics Research Group, INTEC Department, Ghent University-imec, 9000, Ghent, Belgium (phone: +32-9-264-3447; fax: +32-9-264-3593; e-mail: Stevan.Stankovic@intec.ugent.be; Gunther.Roelkens@intec.Ugent.be;).

R. Jones, M. N. Sysak, and J. M. Heck are with Intel Corporation, Santa Clara, CA 95054, USA (e-mail: richard.jones@intel.com; matthew.n.sysak@intel.com; john.heck@intel.com;).

chemical-mechanical polishing (CMP) and wet etching techniques. As the refractive index of SiO_2 at 1310nm (1.45) is similar to the refractive index of DVS-BCB (1.55), this planarized Si rib waveguide exhibits similar optical properties as the standard rib waveguide when immersed in a DVS-BCB bonding layer. This SOI wafer planarization enhances the bonding yield when very thin (<100 nm) DVS-BCB bonding layers need to be achieved. The buried oxide (BOX) layer is 1μm thick. The epitaxial III-V structure, bonded on top of the waveguide, is essentially the same as the one in [10] with a 240nm-thick n-type InP spacer layer and 16.8 μm wide mesa structure comprising 8 quantum wells (QW's) based on InAlGaAs alloys. For a DVS-BCB bonding layer thicknesses between 20 nm and 120 nm, the fundamental hybrid optical transverse electric (TE) polarized mode is predominantly confined within the Si waveguide (Γ_{Si} > 70%), with only a fraction of the optical power within the MQW active region (Γ_{MQW} >3%). The current injection is confined using proton implantation in the lateral sections of the mesa so as to excite the lowest threshold fundamental hybrid mode which is confined to the central part of III-V mesa (see Fig. 1).

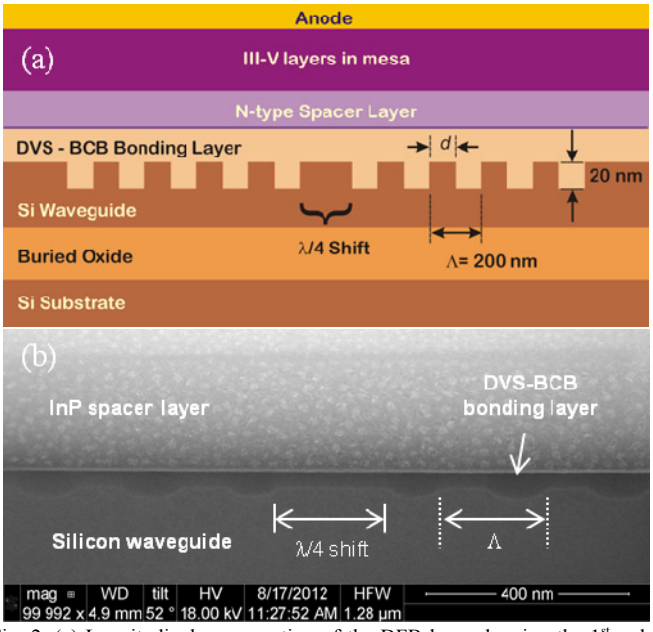

Fig. 2. (a) Longitudinal cross-section of the DFB laser showing the 1st-order grating with the 20nm-deep corrugations on top of Si rib waveguide and λ/4 shift region in the centre of the grating. (b) SEM image of the longitudinal cross-section of the λ/4 shift region in the centre of the grating. Duty cycle of the fabricated grating is 45%, while the thickness of the DVS-BCB bonding layer is ~ 40 nm.

Distributed feedback is provided by corrugations made on top of the Si rib waveguide (see Fig 2a), fabricated by 193nm deep ultraviolet (DUV) lithography. The corrugations are 20 nm deep and designed to form a 1st-order grating for 1310 nm wavelength with a grating period of Λ = 200 nm. The effective indices of the unetched and the etched regions are calculated using the film mode matching (FMM) method and used to calculate the coupling coefficient κ. Dependence of the coupling coefficient κ with respect to the DVS-BCB bonding layer thickness and the grating etch depth is presented in Figure 3. For a 40 nm bonding layer thickness, the effective indices in the unetched and the 20 nm etched regions are 3.2771 and 3.2698, respectively resulting in a coupling coefficient of ~156 cm^{-1}. The total grating length is 350 μm with a λ/4 phase shift in the middle of the grating, in order to break modal degeneracy and insure single mode lasing at the Bragg wavelength. The calculated κ·L value for these devices is 5.46. For the 1st-order grating, the highest coupling coefficient and strongest feedback is achieved with a 50% duty cycle, defined as the ratio of the length of the unetched region on top of the Si waveguide (*d*) to the grating period (Λ), as shown in Fig. 2a. This duty cycle was therefore targeted in the fabricated devices.

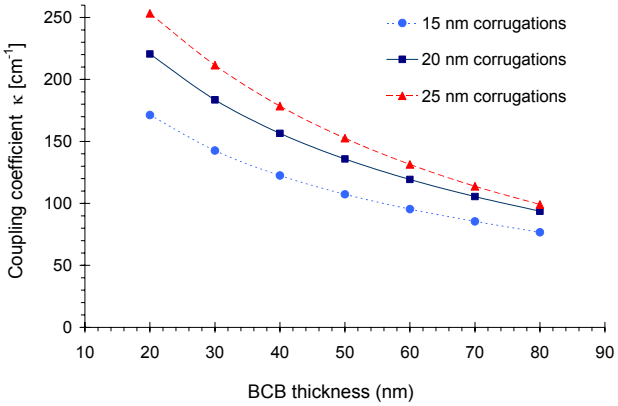

Fig 3. Simulated dependence of the grating coupling coefficient κ on the DVS-BCB bonding layer thickness. The middle curve corresponds to the targeted corrugation depth of 20 nm.

III. Device Fabrication

The first fabrication step is the bonding of an unprocessed III-V die onto an SOI die containing the rib waveguides with gratings. DVS-BCB is spin-coated on the patterned SOI die, brought into contact with the III-V die and subsequently cured. Details of this die-to-die bonding process providing thin (~50nm) DVS-BCB bonding layers are described in [9]. After bonding, the InP substrate is removed by combination of grinding and wet-etching with HCl. A scanning-electron microscope (SEM) image of the longitudinal cross-section of the λ/4-phase shift region in the middle of the grating with the bonded III-V layers is presented in Fig. 2b. The bonding layer thickness can be seen to be around 40 nm and the profile of the corrugations indicates 45% duty cycle grating.

Further processing of the bonded III-V die is similar to that reported in [10]. The III-V islands with mesa structures are defined using contact photolithography and combination of wet and dry etching techniques. Further processing steps include n-type metallization using Au-Ge-Ni alloy, spin-coating and curing a DVS-BCB protective layer, opening windows for p-type contacts in this covering layer and p-type metallization comprising sputtering of a thin Ti layer, followed by deposition of a 1.2 μm-thick Au layer. The thick p-type electrodes act as the mask for subsequent proton implantation which increases electrical resistivity in the lateral

regions of the mesa, confining the injected current to the central region of the mesa. The width of the central p-type electrode (and hence the width of the current confinement window) is 3 μm. After the proton implantation, dry etching is used to open the windows in the covering DVS-BCB layer for n-type contacts. Following this, gold is deposited on both types of electric contacts, for probing. In the final step, dry etching techniques are used to remove the top III-V layers (ohmic contact and p-type top cladding) between the laser and the adjacent monitor photodiode, in order to electrically isolate these regions and enable them to be separately biased. The measured resistance between p-type electrodes isolated in this way is >10 kΩ. Thus, this electrically semi-isolated region (as only p-type contacts are isolated, while n-type contacts remain continuous) acts an integrated evanescent photodetector, sharing the same Si waveguide with the laser. With over 500 μm in length, these photodetectors are sufficiently long to absorb practically all the light emitted by the adjacent DFB laser. A microscope image of a DFB laser with the adjacent integrated photodetector is shown in Fig. 4.

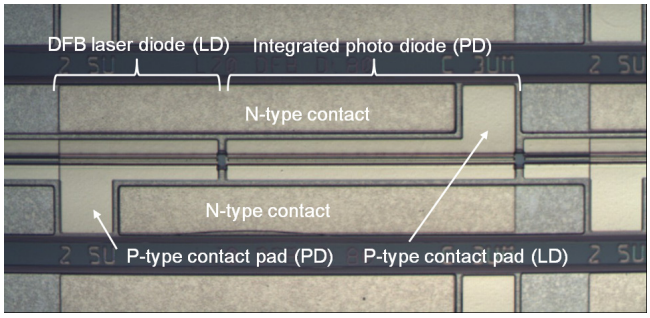

Fig. 4. Microscope image of DFB lasers with the adjacent integrated photodetectors. P-type contacts in the lasers and photodiodes are electrically isolated.

IV. Device Characterization

The chip with the fabricated devices is mounted on a copper plate and its temperature is stabilized using a Peltier element. Photocurrent (I_{ph}) from the photodetector is measured and used to assess the optical output of the laser. Typical I_{ph}-I plots in CW regime, for the temperatures in the range from 10 °C to 55 °C are shown in Fig. 5. The threshold current at 20 °C is 20 mA, which for a 350μm-long laser and assuming a 3μm-wide injection channel corresponds to a threshold current density of 1.9 kA/cm^2. The optical power is assessed based on the detected photocurrents. At 1310 nm wavelength, the maximum responsivity of the integrated photodetectors is 1.05 A/W, assuming 100% quantum efficiency. In order to conservatively estimate the output power of the lasers, we adopt this value. In this way, we conclude that the maximum optical power at 20 °C is 2.1 mW, while the slope efficiency is ~0.026 W/A. At 10 °C, the maximum optical output power rises to 2.85 mW and the slope is ~0.03 W/A. Series resistance of the lasers is around 12 Ω.

The kinks observed in I_{ph}-I curves at lower stage temperatures and higher output optical power levels are similar to those reported by Fang et al. [5] and are attributed to instabilities in the laser optical output caused by the reflections from the corrugations of the adjacent DFB lasers, which are located on the same Si rib waveguide. As the current injection increases, the device heats up and this changes the phase of the reflected light resulting in instabilities in the total optical output.

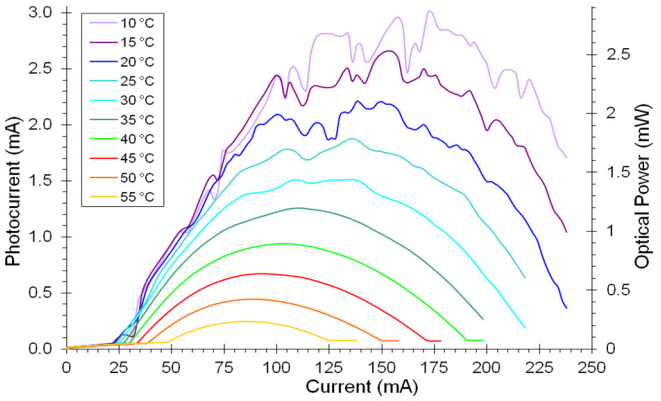

Fig. 5. Detected photocurrent vs. drive current (I_{ph}-I) plots of the hybrid DFB laser in CW regime (in a temperature range from 10 °C to 55 °C). The right axis shows the optical power, estimated using 1.05 A/W responsivity for the integrated photodetector.

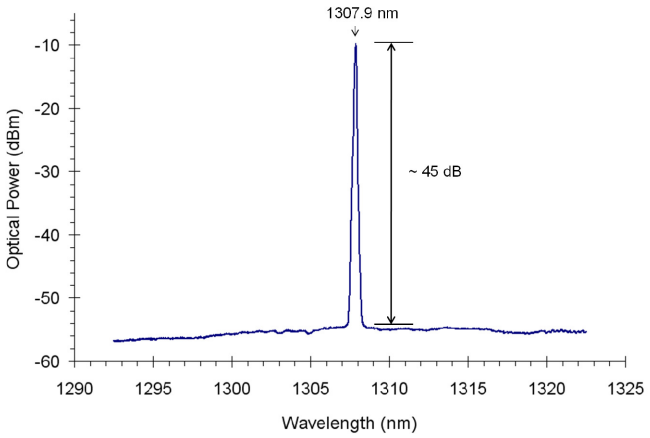

Fig. 6. Optical spectra of the hybrid DFB laser (CW regime, 100 mA injected current).

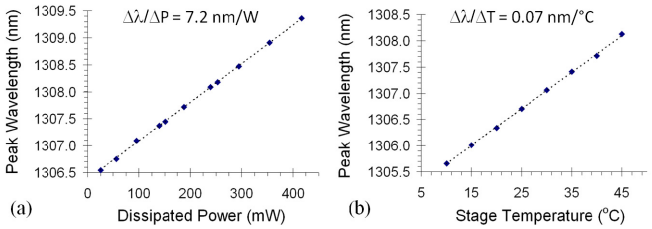

Fig. 7. Peak wavelength shift versus: (a) dissipated power (CW regime) and (b) stage temperature (pulsed regime).

In order to measure the laser emission optical spectrum, the original chip was cleaved into narrow bars, each containing a column of DFB lasers and adjacent photodetectors. The emitted light was collected from the cleaved facet next to a DFB laser and coupled to an optical spectrum analyzer. A typical optical spectrum of the laser in continuous wave (CW) regime, measured with a resolution bandwidth of 0.1 nm, is

given in Fig. 6. The peak wavelength is at 1307.9 nm. The side mode suppression ratio (SMSR) is about 45 dB and the fact that there are no other peaks within the wavelength span of 30 nm, clearly suggest a single-mode lasing characteristic for a quarter-wave-shifted DFB laser. In addition to this, a series of optical spectral measurements in both CW and pulsed regimes were performed in order to measure the thermal impedance (R_{th}) of the device, using the method described in [11]. In CW regime, the observed shift in the peak lasing wavelength ($\Delta\lambda$) was measured versus the dissipated power in the device. In the pulsed regime (1% duty cycle, 100 μs pulse repetition interval), the shift $\Delta\lambda$ was measured versus the temperature of the stage (controlled using a Peltier element). Results of these measurements are shown in Fig. 7. Using a linear fit, we measure the wavelength shift with the increase of dissipated power of $\Delta\lambda/\Delta P$ = 7.2 nm/W, while the wavelength shift with the increase of the temperature of the stage is $\Delta\lambda/\Delta T$ = 0.07 nm/°C. Dividing these values yields a thermal impedance of 102.9 K/W. This value is comparable to thermal impedance of 110.1 K/W that was calculated for a 350μm-long device and 40 nm thick BCB bonding layer, using finite-element method simulation including Joule heating. The higher value obtained from the simulations can be explained by the fact that we excluded conduction through the DVS-BCB covering layer and the convection from the top surface, forcing all the simulated heat flow towards the substrate. The measured thermal impedance of 103 K/W is larger than 41.8 K/W reported for a 850μm-long hybrid III-V/Si laser based on a direct wafer bonding [11]. Given the different device lengths, it is interesting to compare their thermal characteristics per unit length. Instead of comparing device thermal conductivity per unit length, we introduce the inverse of this value as the specific thermal impedance. It is calculated as the product of the device length and the device thermal impedance. The specific thermal impedance of a BCB-bonded laser is 36 K·mm/W, while for a for direct-bonded laser is 35.5 K·mm/W, indicating that per unit length, the performance of these devices is similar. Nevertheless, the strategies for reducing thermal impedance of the device will be pursued in the future work, primarily by adding a thermal via or flip-chipping the fabricated devices upside down on a silicon substrate that serves as a heat sink.

V. Conclusions

We have demonstrated an evanescently coupled, hybrid III-V/silicon DFB laser, based on DVS-BCB adhesive bonding, emitting at 1310 nm. The distributed feedback is realized via 20nm-deep corrugations on top of the Si rib waveguide. The device is fabricated using a specially developed die-to-die DVS-BCB bonding technique, offering more relaxed bonding conditions compared to direct bonding. Single-mode lasing in the CW regime was demonstrated up to 55 °C, with an SMSR value of ~ 45 dB. The relatively low optical power output can be attributed to a high $\kappa \cdot L$ product of 5.46. A possible strategy for lowering this value would be to design DFB lasers with longer phase-shift regions and shorter gratings at both ends, as reported by Srinivasan *et al.* [12]. An increase in the bonding layer thickness would lower the $\kappa \cdot L$ product, but it would also increase the thermal impedance, while further reducing the corrugation depth might negatively affect the SOI wafer fabrication repeatability. A thermal impedance of 103 K/W was estimated from optical spectra measurements, indicating a specific thermal impedance of 36 K·mm/W, which is comparable to the performance of directly-bonded hybrid III-V/Si lasers. Further improving the thermal properties of the lasers will be the subject of the future work. Additionally, the thin DVS-BCB bonding process will be scaled up to bond multiple III-V dies to an SOI wafer, allowing large-scale integration of hybrid lasers on silicon photonic integrated circuits.

Acknowledgment

The authors would like to thank Ran Feldesh and Hanan Bar from Numonyx for SOI wafer fabrication and Steven Verstuyft and Liesbet Van Landschoot of Photonics Research Group of Ghent University for technical assistance in the cleanroom work.

References

[1] A.W. Fang, H. Park, R. Jones, O. Cohen, M. J. Paniccia, and J. E. Bowers, "A Continuous-Wave Hybrid AlGaInAs–Silicon Evanescent Laser," *IEEE Photon. Technol. Lett.*, vol. 18, no. 10, pp. 1143-1145, May 2006.

[2] H.-H. Chang, *et al.*, "1310nm silicon evanescent laser," *Opt. Express*, vol. 15, no.18, pp. 11466-11470, Aug. 2007.

[3] X. Sun, *et al.*, "Electrically pumped hybrid evanescent Si/InGaAsP lasers," *Opt. Lett.*, vol. 34, no.9, pp. 1345-1347, May 2009.

[4] A. W. Fang, *et al.*, "A Distributed Bragg Reflector Silicon Evanescent Laser," *IEEE Photon. Technol. Lett.*, vol. 20(20), pp. 1667-1669,. 2008.

[5] A.W. Fang, E. Lively, Y. Kuo, D. Liang, and J. E. Bowers, "A distributed feedback silicon evanescent laser," *Opt. Express*, vol. 16, no. 7, pp. 4413-4419, Mar. 2008.

[6] G. Roelkens, D. Van Thourhout, R. Baets, R. Notzel, and M. Smit, "Laser emission and photodetection in an InP/InGaAsP layer integrated on and coupled to a Silicon-on-Insulator waveguide circuit" *Opt. Express*, vol. 14, no. 18, pp. 8154-8159, Sept. 2006.

[7] M. Lamponi *et al*, "Low-Threshold Heterogeneously Integrated InP/SOI Lasers With a Double Adiabatic Taper Coupler", *IEEE Photon. Technol. Lett.*, vol. 24, no. 1, pp. 76-78, January 2012.

[8] L. Liu, T. Spuesens, G. Roelkens, D. Van Thourhout, P. Regreny, and P. Rojo-Romeo, "A Thermally Tunable III-V Compound Semiconductor Microdisk Laser Integrated on Silicon-on-Insulator Circuits," *IEEE Photon. Technol. Lett.*, vol. 22, no. 17, pp. 1270-1272, September 2010.

[9] S. Stanković, R. Jones, J. Heck, M. Sysak, D. Van Thourhout, and G. Roelkens, "Die-to-die adhesive bonding for evanescently-coupled photonic devices", *Electrochem. Solid-State Lett.*, vol. 14, no. 8, pp. H326-H329, May 2011.

[10] S. Stanković, R. Jones, M. N. Sysak, J. M. Heck, G. Roelkens, and D. Van Thourhout, "1310-nm Hybrid III–V/Si Fabry–Pérot Laser Based on Adhesive Bonding," *IEEE Photon. Technol. Lett.*, vol. 23, no. 23, pp. 1781-1783, December 2011.

[11] M. N. Sysak *et al.*, "Experimental and theoretical thermal analysis of a Hybrid Silicon Evanescent Laser," *Opt. Express*, vol. 15, no. 23, pp. 15041-15046, Nov. 2007.

[12] S. Srinivasan, A. W. Fang, D. Liang, J. Peters, B. Kaye, and J. E. Bowers, "Design of phase-shifted hybrid silicon distributed feedback lasers," *Opt.Express*, vol. 19, no. 10, pp.9255-9261, May 2011.